Compact mid-infrared dual-comb spectrometer over 3-4 μm via intrapulse difference frequency generation in $LiNbO_3$ waveguide

Lian Zhou[1,#], Haipeng Lou[1,#], Zejiang Deng[1], Xiong Qin[1], Jiayi Pan[1], Yuanfeng Di[1], Chenglin Gu[1], Daping Luo[1,*], and Wenxue Li[1,2,*]

[1]*State Key Laboratory of Precision Spectroscopy, East China Normal University, Shanghai 200062, China*
[2]*Joint Research Center of Light Manipulation Science and Photonic Integrated Chip of East China Normal University and Shandong Normal University, East China Normal University, Shanghai 200241, China*
[*]*dpluo@lps.ecnu.edu.cn; wxli@phy.ecnu.edu.cn*
[#]*These authors contributed equally to this work*

Abstract: Mid-infrared optical frequency comb is a powerful tool for gas sensing. In this study, we demonstrate a simple mid-infrared dual-comb spectrometer covering 3–4 μm in $LiNbO_3$ waveguide. Based on a low-power fiber laser system, the mid-infrared comb is achieved via intra-pulse difference frequency generation in the $LiNbO_3$ waveguide. We construct pre-chirp management before supercontinuum generation to control spatiotemporal alignment for pump and signal pulses. The supercontinuum is directly coupled into a chirped periodically poled $LiNbO_3$ waveguide for the 3–4 μm idler generation. A mid-infrared dual-comb spectrometer based on this approach provides a 100 MHz resolution over 25 THz coverage. To evaluate the applicability for spectroscopy, we measure the methane spectrum using the dual-comb spectrometer. The measured results are consistent with HITRAN database, which the root mean square of the residual is 3.2%.

This peer-reviewed article has been accepted for publication but not yet copyedited or typeset, and so may be subject to change during the production process. The article is considered published and may be cited using its DOI.

10.1017/hpl.2024.2

This proposed method is expected to develop integrated and robust mid-infrared dual-comb spectrometers on chip for sensing.

Key words: nonlinear optics; dual-comb spectroscopy; difference frequency generation; mid-infrared gas sensing

I. Introduction

Optical frequency combs are powerful tools for rapid gas sensing. In particular, frequency comb spectroscopy in the mid-infrared (MIR, 3–5 μm) region of the atmospheric window has made significant progress in various applications, such as greenhouse gas monitoring, atmospheric monitoring, green agriculture, and breath analysis [1–4]. Generally, these MIR frequency combs can be obtained via $\chi^{(2)}$ and $\chi^{(3)}$ nonlinear processes in lithium niobate (LN) [5–9], which is a widely used optical material that can provide wide transparency window, high nonlinear coefficient, and electro-optical effect for integrated chip-based laser devices [10]. In comparison with bulk crystals, periodically poled LN (PPLN) waveguides with strong light confinement ensure high-efficiency nonlinear frequency conversion over a long interaction path. Therefore, PPLN waveguides allow low-power near-infrared (NIR) laser systems to perform efficient nonlinear processes and scale their spectra to the MIR region [11–14]. MIR sources based on LN waveguides have small size and low power consumption, making them ideal for the construction of integrated MIR frequency comb equipment. In addition, the dual-comb spectroscopy (DCS) system can realize high-resolution rapid spectral measurements by employing a single photodetector [15, 16]. DCS combined with the photonic technology can significantly reduce the equipment size and facilitate the development of portable gas sensors. Numerous integrated frequency combs based on microresonators, interband cascade lasers or diode lasers have been demonstrated for spectroscopy [17–19].

MIR spectroscopy offers high sensitivity for molecular sensing. However, limited spectral bandwidth and complex phase control pose two major challenges in demonstrating the technological advantages of DCS in the MIR region. To meet the bandwidth requirements, nonlinear conversion methods have been developed to broaden the spectra to the MIR region, including supercontinuum generation (SCG), difference frequency generation (DFG), and optical parametric oscillators (OPO) [20]. State-of-the-art broadband MIR dual-comb systems have been achieved via DFG and OPO, which have also been successfully applied in comb-line resolved DCS and multispecies detection of trace gases [21–24]. Generally, the DFG system, which can passively stabilize the carrier-envelope phase of the MIR comb, consists of the noncollinear pump and signal branches from the same seed laser. In this two-branch structure, delay control is required to stabilize the pump-signal pulses walk-off in the time domain and suppress the intensity noise of MIR pulses [25]. Recently, several studies have reported the simple method of MIR comb generation via intra-pulse DFG (IPDFG) [26–30]. Through precise chirp management of the supercontinuum, a single branch can provide natural spatiotemporal alignment for the pump and signal pulses, achieving multi-octave-spanning MIR combs [26–28]. The potential of these simple

https://doi.org/10.1017/hpl.2024.2 Published online by Cambridge University Press

IPDFG MIR systems for high-resolution DCS has been demonstrated in the past [29, 30]. By combining the IPDFG and PPLN waveguides, a broadband MIR comb source was realized with an integrated and simple structure [31]. Therefore, we believe that a portable gas-sensing instrument can be developed using DCS and IPDFG combs on a LN waveguide.

In this study, a simple 3–4 μm MIR dual-comb spectrometer with waveguide-based IPDFG modules is demonstrated. We constructed an Er-doped fiber dual-comb system as the seed source. To realize the spatiotemporal alignment of the pump and signal pulses, the front prism pair provides easily adjustable pre-chirp control for the soliton self-compression in a highly nonlinear fiber (HNLF). The broadband MIR combs over the 3–4 μm region were yielded from high-efficiency chirped PPLN waveguides via the IPDFG process. Thereafter, the comb-line-resolved DCS with 100 MHz spectral resolution over 25 THz coverage was demonstrated. Finally, we measured the absorption spectrum of methane to verify the applicability of the MIR dual-comb system for precision spectroscopy. We compared the measured result with the HITRAN database, and the root mean square (RMS) of the residual is 3.2%. This dual-comb system without phase correction enables mode-resolved DCS with a figure of merit of 1.03×10^{6}. Thus far, femtosecond lasers, frequency combs, amplifiers, and SCG on chips have been successfully demonstrated [32–34]. The MIR comb generation method, which does not require the detection of offset frequency of MIR pulses, is conducive to low-power sources on chips. We believe that this approach contributes to the development of broadband MIR frequency combs and portable DCS systems on chips.

II. Experimental setup and results

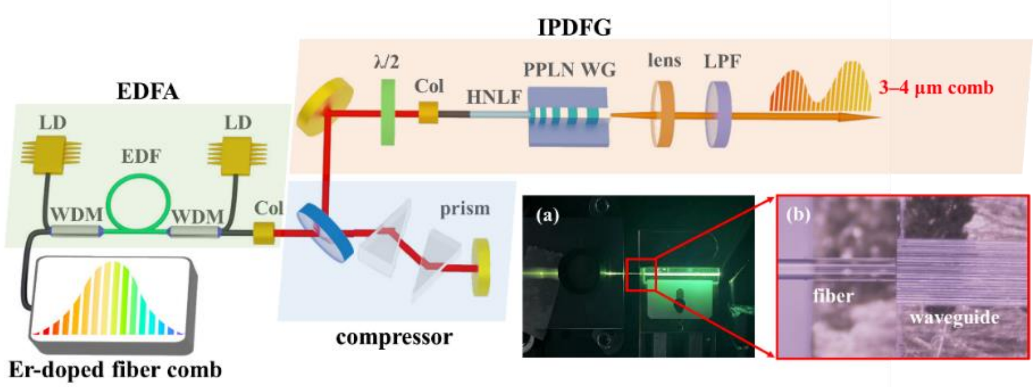

Fig. 1. Schematic of the MIR comb generation. The lens after the waveguide to make the schematic look easier to understand. In the actual system, we use an off-axis parabolic mirror to collimate the MIR light instead of the lens. LD: laser diode; EDF, Er-doped fiber; WDM, wavelength division multiplexer; Col: collimator; EDF, Er-doped fiber amplifier; λ/2, half-

https://doi.org/10.1017/hpl.2024.2 Published online by Cambridge University Press

wave plate; HNLF, highly nonlinear fiber; PPLN WG, periodically poled lithium niobate waveguide; and LPF, long-pass filter. Moreover, we also recorded the images of the PPLN WG using a phone camera (insert a) and a CCD camera (insert b).

The schematic of the MIR comb generation is shown in Figure 1, which includes a seed comb centered at 1.5 μm, Er-doped fiber amplifier, prism compressor, HNLF, and IPDFG module. The seed comb based on an Er-doped fiber mode-locked laser emitted a pulse train with a 1 mW average power and a 100 MHz repetition rate. The average pulse power was scaled up to 328 mW using a bidirectionally pumped fiber amplifier, in which a 3 m Er-doped single-mode fiber with a normal dispersion was used as the gain medium. A pair of silicon prisms was adopted to provide controllable anomalous dispersion for pre-chirp management of SCG. Linearly polarized light was injected into the dispersion prisms at a Brewster angle to reduce the reflection loss on the prism surfaces. Behind the prism compression, 300 mW laser was coupled to a collimator with 12 cm PM1550 pigtail fiber, which could further recompress the pulse duration. Figure 2(a) and (b) are the autocorrelation curve and spectrum after the prism compressor respectively. The pulse duration is 92 fs with $sech^2$ fitting, and the spectrum covers the range from 1520 nm to 1620 nm. The large pulse wings are caused by uncompensated nonlinear chirp. 3 cm PM HNLF with an anomalous dispersion of 1.9 ps/(nm·km) was employed to generate a supercontinuum spectrum. The spectral broadening and soliton self-compression processes in the anomalous-dispersion HNLF were adjusted using the prism-based pre-chirp management module.

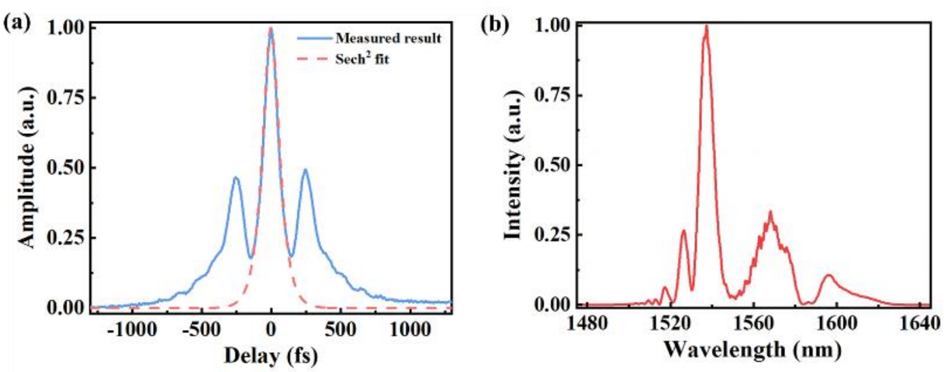

Fig. 2. (a) Autocorrelation trace and (b) Measured spectrum of the compressor output.

To drive the IPDFG and yield MIR light, the supercontinuum from the HNLF was directly coupled to a chirped PPLN waveguide. The HNLF is placed on a 3-axis stage to launch light to the waveguide. A zoom lens and camera system on the top of the waveguide were used for high-magnification imaging. By adjusting the stage, we can get the optimal alignment and measure the output light. The mode diameter of HNLF is 3.5 μm. This PPLN waveguide is 15 μm wide and 25 mm long with aperiodic periods of 23–32 μm that were consistent with our previous study [35]. The coupling efficiency is 60%. In general, some spatial optical components, including wedge and chirp mirrors, were required to control the pulse chirp before IPDFG [26, 28]. These extra spatially manipulated modules increased total loss and system complexity. In particular, we did not adopt common methods for controlling the chirp but simply adjusted the prism pair before the anomalous-dispersion HNLF to optimize the temporal alignment of pump-signal pulses with the

https://doi.org/10.1017/hpl.2024.2 Published online by Cambridge University Press

soliton self-compression effect [27, 36–38]. In addition, these prisms could be removed completely to simplify the system for integrated MIR comb generation [31]. Thereafter, a gold-coated off-axis parabolic mirror with a focal distance of 6 mm collimated the light to free space. Finally, a long-pass filter at 2.4 μm was used to filter out the residual pump and signal light, outputting MIR frequency comb with a high transmissivity.

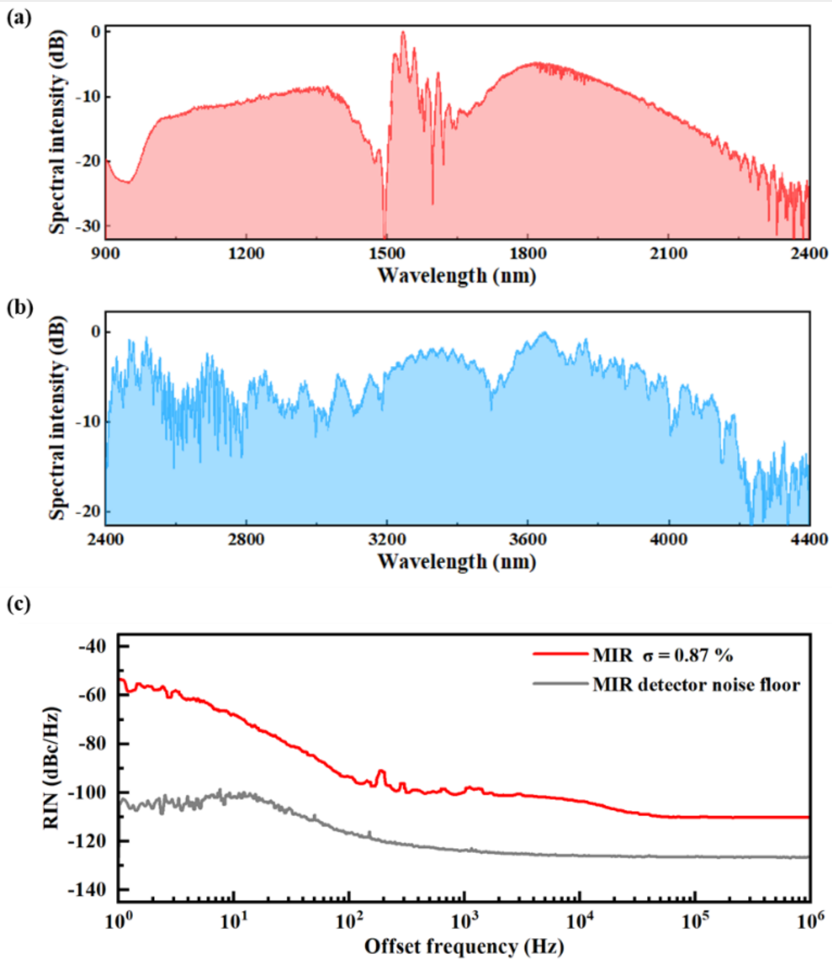

Fig. 3. (a) Spectral profile of SCG. The spectral region is separately measured using Yokogawa AQ6370 (900–1700 nm) and Bristol 771B (1700–2400 nm). (b) The spectral profile of the MIR comb. (c) The RIN of MIR light.

To characterize the spectral evolution of the SCG and IPDFG, we measured the corresponding spectral profiles using two commercial spectrometers (Yokogawa AQ6370 and Bristol 771B). The HNLF delivers 150 mW supercontinuum with a spectral range of 1-2 μm, as shown in Fig. 3(a). Theoretically, this supercontinuum spectrum can provide the pump and signal light for 2–5 μm idler generation. In addition, absorption lines were observed at approximately 1900 nm owing to water vapor in the air. To maximize the conversion efficiency of the IPDFG, the slow axis of the HNLF was rotated to ensure that the pump and signal lights were coupled to the waveguide with vertical polarization. After the filter, 0.7 mW MIR light was obtained. The spectrum was measured

https://doi.org/10.1017/hpl.2024.2 Published online by Cambridge University Press

using a Fourier-transform spectrometer (Bristol 771 B) with a 33 GHz spectral resolution, as shown in Fig. 3(b). We observed that the long wavelength was cut off at 4.2 μm, which was not as broad as expected. The most likely reason is that the waveguide channel brought different group velocity dispersions to the pump and signal pulses, which caused temporal misalignment of the pump and signal pulses. In addition, the effect of waveguide dispersion on the refractive index is ignored, so the poling periods are not optimal. In future studies, dispersion engineering and poling periods should be considered to redesign the waveguide and broaden the MIR spectrum [39]. We measured the relative intensity noise (RIN) of MIR light, as shown in Fig. 3(c). The integrated RIN is 0.87%.

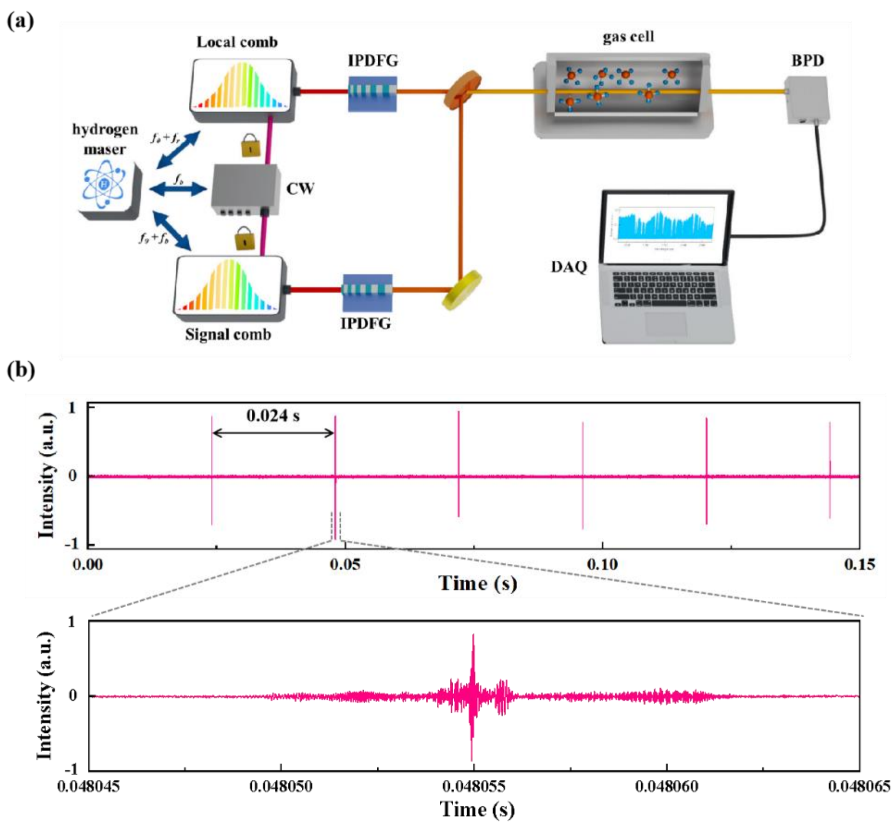

Fig. 4. (a) Schematic of the MIR dual-comb system. The recorded interferograms at different time scales of (b) 150 and (c) 0.02 ms. CW: continuous laser; BPD, balanced photodetector; DAQ, data acquisition.

A dual-comb spectrometer based on the IPDFG method was constructed for DCS measurement, as shown in Fig. 4(a). Two Er-doped fiber comb systems served as the seed combs. The NIR local comb (f_{0_comb1} = 20 MHz and f_{r_comb1} = 100 MHz) was referenced to the hydrogen maser clock. A 10 Hz linewidth CW laser centered at 1560 nm (OE4030, OEwaves) was referenced to the local comb to provide a standard optical frequency reference for the signal comb. To stabilize the signal comb, the carrier-envelope-phase offset frequency (f_{0_comb2} = 20 MHz) and the optical beat note were locked. Moreover, two electro-optic modulators were used in the signal oscillator to improve

https://doi.org/10.1017/hpl.2024.2 Published online by Cambridge University Press

the modulation bandwidth of the frequency control [40]. Thereafter, two combs were delivered into two parallel IPDFG modules to generate the MIR dual-comb system. The two MIR combs could provide a broad spectrum from 2.4 to 4.2 μm. To evaluate the applicability for spectroscopy, the two MIR beams were combined to pass through an 8 cm gas cell filled with pure methane at a pressure of 150 mbar. The interferogram signal was acquired through a balanced photodetector (Qube-DT, ppqSense) equipped with two HgCdTe photodetectors (PVI-2TE-5, VIGO System). The response spectral range of the detector is 3–5 μm. In addition, two half-wavelength plates were used to control the polarization of the MIR light and optimize the signal-to-noise ratio (SNR) of the interferograms. Before the detection, we attenuated the power of the signal comb to ensure that the two beams with the same power were injected into the detector. After passing through a 48 MHz electronic low-pass filter, the DCS signal was recorded using a data acquisition card with a sampling rate of 100 MHz. Figure 4(b) shows the measured interferogram signal for 150 ms. It is evident that the period of the interferograms was ~0.024 s, corresponding to the repetition rate difference of ~42 Hz. Figure 4(c) exhibits a 0.02 ms temporal domain of interferograms in which we can acquire the information in the frequency domain via further Fourier transform.

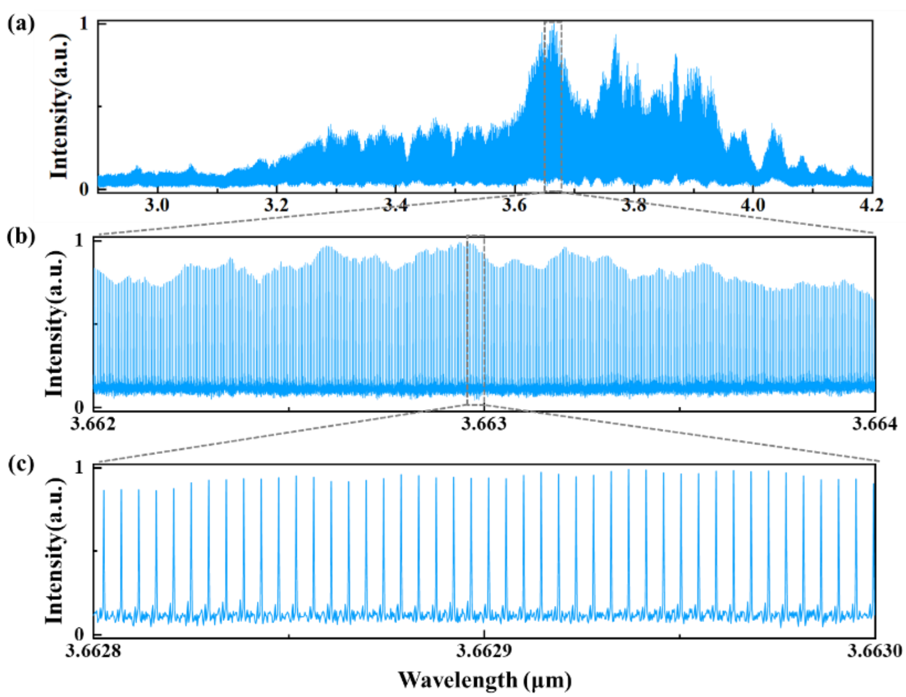

Fig. 5. Mode-resolved MIR dual-comb spectra at different wavelength scales of (a) 1.4, (b) 0.002, and (c) 0.0002 μm.

To retrieve the frequency-domain optical spectrum, 20 interferograms (0.5-s temporal signal) were extracted as a unit for the Fourier transform. A total of 100 s of data were recorded and coherently averaged to obtain a high SNR DCS. As illustrated in Fig. 5(a), we obtained the DCS in the range of 3.0–4.2 μm, corresponding to a frequency bandwidth of 25 THz. The retrieved dual-comb spectrum was narrower than the spectrum measured using a Fourier transform spectrometer

https://doi.org/10.1017/hpl.2024.2 Published online by Cambridge University Press

because we could not retrieve the spectrum in the 2–3 μm range owing to the limited response bandwidth (3–5 μm) of the detector. In the frequency domain, approximately 2.5×10^5 modes were resolved with a 100 MHz spectral resolution. We also calculated the figure of merit, defined as SNR × M / $T^{1/2}$, where M is the number of comb teeth and T is the measurement time. The figure of merit was 1.03×10^6, which is the same order of magnitude as the results in references [30, 41]. In addition, the SNR of the peak spectrum, which represents the ratio of the signal to random variations of the baseline [21], was 28. Figures 5(b) and 5(c) show the mode-resolved MIR dual-comb spectra over wavelength spans of 0.002 and 0.0002 μm, respectively, confirming that the simple DCS system has the capacity for high-resolution gas sensing in the MIR region.

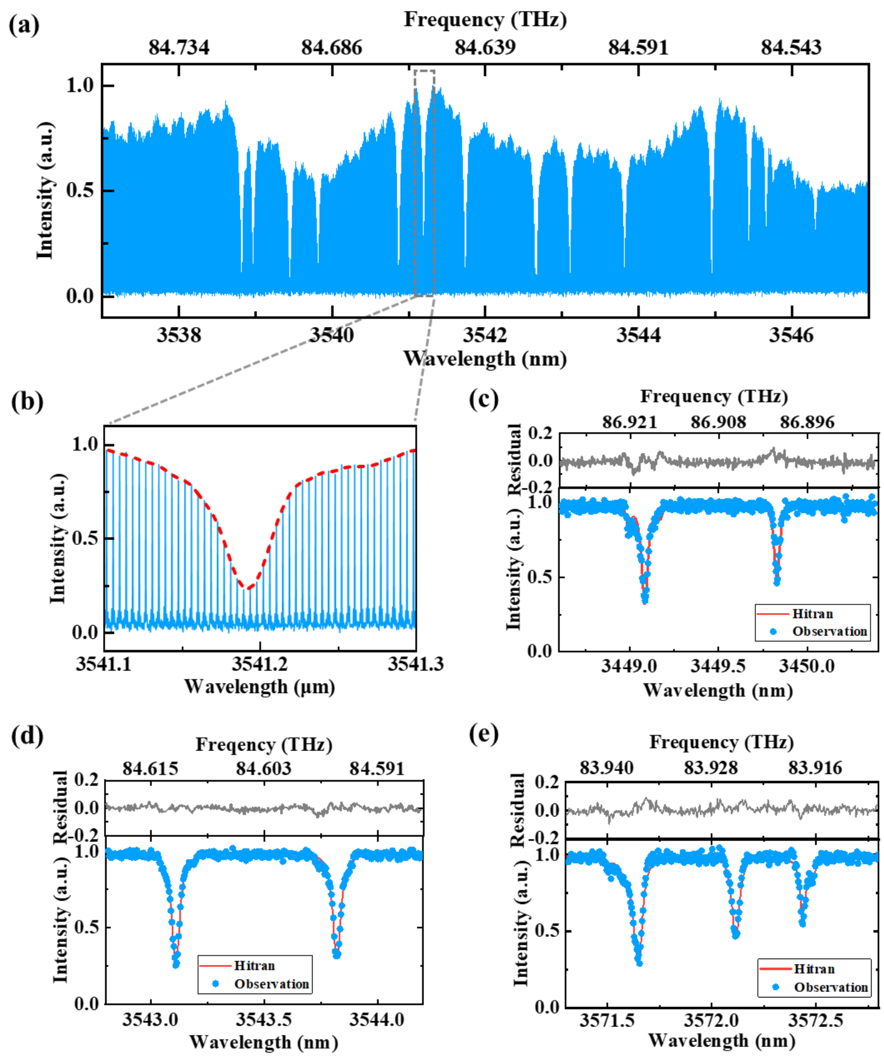

Fig. 6. (a) Absorption lines of methane at 3537–3547 nm region. (b) Zoom-in absorption line of methane at 3541.1–3541.3 nm. (c)–(e) Comparison results of the extracted gas absorption lines (blue dot) and the theoretical profiles from the HITRAN database (red line).

https://doi.org/10.1017/hpl.2024.2 Published online by Cambridge University Press

To assess the applicability of the MIR dual-comb system to high-resolution spectroscopy, we measured its methane absorption spectrum. Several absorption lines in the 3537–3547 nm region is shown in Fig. 6(a). A single absorption peak zoom-in in the 3541.1–3541.3 nm consists of ~50 comb modes with a frequency interval of ~100 MHz, as shown in Fig. 6(b). Figures 6(c)–(e) show several absorption peaks (blue dots), in which all the absorption lines are consistent with the standard profiles (red curves, Voigt profiles, HITRAN 2020 [42]). The RMS of the residuals in Fig. 6(c)–(e) were 3.2%, 1.9% and 2.9%.

In the low SNR range, it is difficult to retrieve the absorption lines. Although the SNR of our system can be further improved by increasing the power. The saturation power (~2 mW) of the detector limited the SNR because each comb line has only nW level power. It remains a challenge for dual-comb systems to achieve high SNR DCS in broadband parallel measurement. Recent work has demonstrated a method of signal processing to resolve this issue in the NIR region, and the ideas could be used to improve the SNR of MIR DCS [43]. In this system, the spectrum has a fast baseline with tens of gigahertz linewidth, which is similar linewidth with the gas absorption line at standard or high atmospheric pressure. So, we measure the gas absorption peak at low pressure (150 mbar) to reduce the impact of the baseline. For broader absorption lines at standard atmospheric pressure, four-point normalization correction method can be used to effectively remove the effects of the baseline [1, 41, 44].

III. Conclusion

We demonstrated a simple and compact MIR dual-comb spectrometer. Using the IPDFG method, we yielded broad MIR combs on chirped PPLN waveguides and developed a mode-resolved dual-comb spectrometer. The spectrometer provided 100 MHz resolution in the range of 3.0–4.2 μm corresponding to 25 THz bandwidth. In comparison with bulky two-branch DFG combs, the proposed MIR comb system is not only more integrated but also more stable, without noise from the pump-signal delay jitter. The high-efficiency PPLN waveguide reduced the power threshold required to drive the IPDFG process. In addition, the lens group for waveguide coupling could be replaced by an all-fiber structure. Optimization of the period distribution and channel length of the waveguide would improve the MIR spectral bandwidth. This MIR dual-comb system is expected to develop into more integrated measurement devices with on-chip femtosecond pulse generation, amplifiers, and nonlinear broadening technologies for portable gas-sensing equipment with high sensitivity and high resolution.

Acknowledgement

This work was supported in part by the National Natural Science Foundation of China (12204178, 12104162, 12134004 and 12274141).

References

1. G. Ycas, F. R. Giorgetta, K. C. Cossel, E. M. Waxman, E. Baumann, N. R. Newbury, and I. Coddington, "Mid-infrared dual-comb spectroscopy of volatile organic compounds across long open-air paths," Optica **6**(2), 165-168 (2019).
2. F. R. Giorgetta, J. Peischl, D. I. Herman, G. Ycas, I. Coddington, N. R. Newbury, and K. C. Cossel, "Open-Path Dual-Comb Spectroscopy for Multispecies Trace Gas Detection in the 4.5–5 μm Spectral Region," Laser Photonics Rev. **15**(9), 2000583 (2021).
3. D. I. Herman, C. Weerasekara, L. C. Hutcherson, F. R. Giorgetta, K. C. Cossel, E. M. Waxman, G. M. Colacion, N. R. Newbury, S. M. Welch, B. D. DePaola, I. Coddington, E. A. Santos, and B. R. Washburn, "Precise multispecies agricultural gas flux determined using broadband open-path dual-comb spectroscopy," Sci Adv. **7**(14), eabe9765 (2021).
4. Q. Liang, Y.-C. Chan, J. Toscano, K. K Bjorkman, L.A Leinwand, R. Parker, E. S Nozik, D. J. Nesbitt, J. Ye, "Breath analysis by ultra-sensitive broadband laser spectroscopy detects SARS-CoV-2 infection," J. Breath Res. **17**(3), 036001 (2023).
5. D. L. Maser, G. Ycas, W. I. Depetri, F. C. Cruz, and S. A. Diddams, "Coherent frequency combs for spectroscopy across the 3–5 μm region," Appl. Phys. B **123**, 142 (2017).
6. F. C. Cruz, D. L. Maser, T. Johnson, G. Ycas, A. Klose, F. R. Giorgetta, I. Coddington, and S. A. Diddams, " Mid-infrared optical frequency combs based on difference frequency generation for molecular spectroscopy," Opt. Express **23**(20), 26814-26824 (2015).
7. L. Nitzsche, J. Goldschmidt, J. Kiessling, S. Wolf, F. Kühnemann, and J. Wöllenstein, "Tunable dual-comb spectrometer for mid-infrared trace gas analysis from 3 to 4.7 μm," Opt. Express **29**(16), 25449-25461 (2021).
8. G. Soboń, T. Martynkien, P. Mergo, L. Rutkowski, and A. Foltynowicz, "High-power frequency comb source tunable from 2.7 to 4.2 μm based on difference frequency generation pumped by an Yb-doped fiber laser," Opt. Lett. **42**(9), 1748-1751 (2017).
9. C. P. Bauer, S. L. Camenzind, J. Pupeikis, B. Willenberg, C. R. Phillips, and U. Keller, "Dual-comb optical parametric oscillator in the mid-infrared based on a single free-running cavity," Opt. Express **30**(11), 19904-19921 (2022).
10. A. Boes, L. Chang, C. Langrock, M. Yu, M. Zhang, Q. Lin, M. Lončar, M. Fejer, J. Bowers, and A. Mitchell, "Lithium niobate photonics: Unlocking the electromagnetic spectrum," Science **379**(6627), eabj4396 (2023).
11. J. Lu, J. B. Surya, X. Liu, Y. Xu, and H. X. Tang, "Octave-spanning supercontinuum generation in nanoscale lithium niobate waveguides," Opt. Lett. **44**(6), 1492-1495 (2019).
12. H. Guo, B. Zhou, X. Zeng, and M. Bache, "Highly coherent mid-IR supercontinuum by self-defocusing solitons in lithium niobate waveguides with all-normal dispersion," Opt. Express **22**(10), 12211-12225 (2014).
13. A. S. Kowligy, A. Lind, D. D. Hickstein, D. R. Carlson, H. Timmers, N. Nader, F. C. Cruz, G. Ycas, S. B. Papp, and S. A. Diddams, "Mid-infrared frequency comb generation via cascaded quadratic nonlinearities in quasi-phase-matched waveguides," Opt. Lett. **43**(8), 1678-1681 (2018).
14. M. Liu, R. M. Gray, L. Costa, C. R. Markus, A. Roy, and A. Marandi, "Mid-infrared cross-comb spectroscopy," Nat Commun **14**(1), 1044 (2023).
15. N. Picqué, and T.W. Hänsch, "Frequency comb spectroscopy," Nat. Photonics **13**(3), 146-157 (2019).

16. I. Coddington, N. Newbury, and W. Swann, “Dual-comb spectroscopy,” Optica **3**(4), 414-426 (2016).
17. C. Bao, Z. Yuan, L. Wu, M.-G. Suh, H. Wang, Q. Lin, and K. J. Vahala, “Architecture for microcomb-based GHz-mid-infrared dual-comb spectroscopy,” Nat Commun **12**, 6573 (2021).
18. L. A. Sterczewski, T.-L. Chen, D. C. Ober, C. R. Markus, C. L. Canedy, I. Vurgaftman, C. Frez, J. R. Meyer, M. Okumura, and Mahmood Bagheri, “Cavity-Enhanced Vernier Spectroscopy with a Chip-Scale Mid-Infrared Frequency Comb,” ACS Photonics **9**(3), 994-1001 (2022).
19. L. A. Sterczewski, M. Fradet, C. Frez, S. Forouhar, and M. Bagheri, “Battery-Operated Mid-Infrared Diode Laser Frequency Combs,” Laser Photonics Rev **17**(1), 2200224 (2022).
20. M. L. Weichman, P. B. Changala, J. Ye, Z. Chen, M. Yan, and N. Picqué, “Broadband molecular spectroscopy with optical frequency combs,” Journal of Molecular Spectroscopy **355**, 66-78 (2019).
21. G. Ycas, F. R. Giorgetta, E. Baumann, I. Coddington, D. Herman, S. A. Diddams, and N. R. Newbury, “High-coherence mid-infrared dual-comb spectroscopy spanning 2.6 to 5.2 μm,” Nat. Photonics **12**(4), 202-208 (2018).
22. A. V. Muraviev, V. O. Smolski, Z. E. Loparo, and K. L. Vodopyanov, “Massively parallel sensing of trace molecules and their isotopologues with broadband subharmonic mid-infrared frequency combs,” Nat. Photonics **12**(4), 209–214 (2018).
23. S. Vasilyev, A. Muraviev, D. Konnov, M. Mirov, V. Smolski, I. Moskalev, S. Mirov, and K. Vodopyanov, "Longwave infrared (6.6–11.4 μm) dual-comb spectroscopy with 240,000 comb-mode-resolved data points at video rate," Opt. Lett. **48**(9), 2273-2276 (2023).
24. T. Tomberg, A. Muraviev, Q. Ru, and K. L. Vodopyanov, "Background-free broadband absorption spectroscopy based on interferometric suppression with a sign-inverted waveform," Optica **6**(2), 147-151 (2019)
25. V. S. Oliveira, A. Ruehl, P. Masłowski, and I. Hartl, “Intensity noise optimization of a mid-infrared frequency comb difference-frequency generation source,” Opt. Lett. **45**(7), 1914-1917 (2020).
26. D. M. B. Lesko, H. Timmers, S. Xing, A. Kowligy, A. J. Lind, and S. A. Diddams, “A six-octave optical frequency comb from a scalable few-cycle erbium fibre laser,” Nat. Photonics **15**(4), 281-286 (2021).
27. S. Xing, D. M. B. Lesko, T. Umeki, A. J. Lind, N. Hoghooghi, T. -H. Wu, and S. A. Diddams, “Single-cycle all-fiber frequency comb,” APL Photonics **6**, 086110 (2021).
28. N. Hoghooghi, S. Xing, P. Chang, D. Lesko, A. Lind, G. Rieker, and S. Diddams, “Broadband 1-GHz mid-infrared frequency comb,” Light Sci. Appl. **11**(1), 264 (2022).
29. A. J. Lind, A. Kowligy, H. Timmers, F. C. Cruz, N. Nader, M. C. Silfies, T. K. Allison, and S. A. Diddams, “Mid-Infrared frequency comb generation and spectroscopy with few-cycle pulses and $\chi(2)$ nonlinear optics,” Phys. Rev. Lett. **124**(13), 133904 (2020).
30. H. Timmers, A. Kowligy, A. Lind, F. C. Cruz, N. Nader, M. Silfies, G. Ycas, T. K. Allison, P. G. Schunemann, S. B. Papp, and S. A. Diddams, “Molecular fingerprinting with bright, broadband infrared frequency combs,” Optica **5**(6), 727-732 (2018).

31. K. Iwakuni, S. Okubo, O. Tadanaga, H. Inaba, A. Onae, F.-L. Hong, and H. Sasada, "Generation of a frequency comb spanning more than 3.6 octaves from ultraviolet to mid infrared," Opt. Lett. **41**(17), 3980-3983 (2016).
32. M. Yu, D. Barton III, R. Cheng, C. Reimer, P. Kharel, L. He, L. Shao, D. Zhu, Y. Hu, H. R. Grant, L. Johansson, Y. Okawachi, A. L. Gaeta, M. Zhang and M. Lončar, "Integrated femtosecond pulse generator on thin-film lithium niobate," Nature **612**(7939), 252-258 (2022).
33. J. Zhou, Y. Liang, Z. Liu, W. Chu, H. Zhang, D. Yin, Z. Fang, R. Wu, J. Zhang, W. Chen, Z. Wang, Y. Zhou, M. Wang, and Y. Cheng, "On-Chip Integrated Waveguide Amplifiers on Erbium-Doped Thin-Film Lithium Niobate on Insulator," Laser & Photonics Reviews **15**(8), 2100030 (2021).
34. B. Kuyken, T. Ideguchi, S. Holzner, M. Yan, T. W. Hänsch, J. V. Campenhout, P. Verheyen, S. Coen, F. Leo, R. Baets, G. Roelkens, and N. Picqué, "An octave-spanning mid-infrared frequency comb generated in a silicon nanophotonic wire waveguide," Nat. Communications **6**(1), 6310 (2015).
35. L. Zhou, Y. Liu, H. Lou, Y. Di, G. Xie, Z. Zhu, Z. Deng, D. Luo, C. Gu, H. Chen, and W. Li, "Octave mid-infrared optical frequency comb from Er:fiber-laser-pumped aperiodically poled Mg: $LiNbO_3$," Opt. Lett. **45**(23), 6458-6461 (2020).
36. J. C. Travers, T. F. Grigorova, C. Brahms, and F. Belli, "High-energy pulse self-compression and ultraviolet generation through soliton dynamics in hollow capillary fibres," Nat. Photonics **13**(8), 547-554 (2019).
37. S. Xing, A. S. Kowligy, D. M. B. Lesko, A. J. Lind, and S. A. Diddams, "All-fiber frequency comb at 2 μm providing 1.4-cycle pulses," Opt. Lett. **45**(9), 2660-2663 (2020).
38. Z. Li, C. Yao, Z. Jia, F. Wang, G. Qin, Y. Ohishi, and W. Qin, "Broadband supercontinuum generation from 600 to 5400 nm in a tapered fluorotellurite fiber pumped by a 2010 nm femtosecond fiber laser", Appl. Phys. Lett. **115**(9), 091103 (2019).
39. M. Jankowski, C. Langrock, B. Desiatov, A. Marandi, C. Wang, M. Zhang, C. R. Phillips, M. Lončar, and M. M. Fejer, "Ultrabroadband nonlinear optics in nanophotonic periodically poled lithium niobate waveguides," Optica **7**(1), 40-46 (2020).
40. Z. Deng, Y. Liu, Z. Zhu, D. Luo, C. Gu, L. Zhou, G. Xie, and W. Li, "Ultra-precise optical phase-locking approach for ultralow noise frequency comb generation," Opt. Laser Technol. **138**, 106906 (2021).
41. G. Ycas, F. R. Giorgetta, J. T. Friedlein, D. Herman, K. C. Cossel, E. Baumann, N. R. Newbury, and I. Coddington, "Compact mid-infrared dual-comb spectrometer for outdoor spectroscopy," Opt. Express **28**, 14740-14752 (2020).
42. I. E. Gordon, L. S. Rothman, R. J. Hargreaves, R. Hashemi, E. V. Karlovets, F. M. Skinner, E. K. Conway, C. Hill, R. V. Kochanov, Y. Tan, P. Wcisło, A. A. Finenko, K. Nelson, P. F. Bernath, M. Birk, V. Boudon, A. Campargue, K. V. Chance, A. Coustenis, B. J. Drouin, J. –M. Flaud, R. R. Gamache, J. T. Hodges, D. Jacquemart, E. J. Mlawer, A. V. Nikitin, V. I. Perevalov, M. Rotger, J. Tennyson, G. C. Toon, H. Tran, V. G. Tyuterev, E. M. Adkins, A. Baker, A. Barbe, E. Canè, A. G. Császár, A. Dudaryonok, O. Egorov, A. J. Fleisher, H. Fleurbaey, A. Foltynowicz, T. Furtenbacher, J. J. Harrison, J. –M. Hartmann, V. –M. Horneman, X. Huang, T. Karman, J. Karns, S. Kassi, I. Kleiner, V. Kofman, F. Kwabia–Tchana, N. N. Lavrentieva, T. J. Lee, D. A. Long, A. A. Lukashevskaya, O. M. Lyulin, V. Yu. Makhnev, W. Matt, S. T.

https://doi.org/10.1017/hpl.2024.2 Published online by Cambridge University Press

Massie, M. Melosso, S. N. Mikhailenko, D. Mondelain, H. S. P. Müller, O. V. Naumenko, A. Perrin, O. L. Polyansky, E. Raddaoui, P. L. Raston, Z. D. Reed, M. Rey, C. Richard, R. Tóbiás, I. Sadiek, D. W. Schwenke, E. Starikova, K. Sung, F. Tamassia, S. A. Tashkun, J. Vander Auwera, I. A. Vasilenko, A. A. Vigasin, G. L. Villanueva, B. Vispoel, G. Wagner, A. Yachmenev, and S. N. Yurchenko, "The HITRAN2020 molecular spectroscopic database," Journal of Quantitative Spectroscopy and Radiative Transfer **277**, 107949 (2022).

43. Philippe Guay, Mathieu Walsh, Alex Tourigny-Plante, and Jérôme Genest, "Linear dual-comb interferometry at high power levels," Opt. Express **31**, 4393-4404 (2023).
44. G. B. Rieker, F. R. Giorgetta, W. C. Swann, J. Kofler, A. M. Zolot, L. C. Sinclair, E. Baumann, C. Cromer, G. Petron, C. Sweeney, P. P. Tans, I. Coddington, and N. R. Newbury, "Frequency-comb-based remote sensing of greenhouse gases over kilometer air paths," Optica **1**(5), 290-298 (2014).